We are IntechOpen,
the world's leading publisher of
Open Access books
Built by scientists, for scientists

6,900
Open access books available

185,000
International authors and editors

200M
Downloads

154
Countries delivered to

Our authors are among the

TOP 1%
most cited scientists

12.2%
Contributors from top 500 universities

CLARIVATE ANALYTICS
BOOK CITATION INDEX
INDEXED

WEB OF SCIENCE™

Selection of our books indexed in the Book Citation Index
in Web of Science™ Core Collection (BKCI)

Interested in publishing with us?
Contact book.department@intechopen.com

Numbers displayed above are based on latest data collected.
For more information visit www.intechopen.com

Analysis of the Precipitation and Growth Processes of the Intermetallic Phases in an Fe-Ni Superalloy

Kazimierz J. Ducki

Abstract

The chapter characterizes wrought iron-base superalloys and comprises two main parts. The first describes the chemical composition, microstructure, and precipitation reactions in Fe-Ni, Ni-Fe, and Fe-Cr superalloys. The second part presents the influence of prolonged aging on the precipitation and growth processes in an Fe-Ni superalloy of A-286 type. The prepared specimens, after solution heat treatment at 980°C/2 h/water, were aged at temperatures of 715°C, 750°C, and 780°C with the holding time of 0.5-500 h. Transmission electron microscopy (TEM) and X-ray diffraction were used to examine their structures. It was found, that application of a single-stage aging causes precipitation processes of γ' - Ni$_3$(Al,Ti), η - Ni$_3$Ti, β - NiTi, G - Ni$_{16}$Ti$_6$Si$_7$, and σ - Cr$_{0.46}$Mo$_{0.40}$Si$_{0.14}$ intermetallic phases, as well as the carbide M$_{23}$C$_6$ and boride M$_3$B$_2$. The main phase precipitating during alloy aging was the γ'-type intermetallic phase. It was found that the mean diameter of γ' phase precipitates increases as a function of the cube root of aging time, which is consistent with the predictions based on the Lifshitz-Slyozow-Wagner (LSW) theory. The determined value of activation energy for the process of γ' phase coagulation in the examined alloy was E = 297 kJ/mole.

Keywords: A-286 alloy, Precipitation and growth, Intermetallic phases, LSW theory

1. Introduction

High-temperature Fe-Ni superalloys after precipitation strengthening with intermetallic phases have a number of characteristic properties, including excellent mechanical properties,

good creep and heat resistance at elevated and high temperatures. They also show very good corrosion resistance, as well as high ductility at low temperatures, and are non-magnetic. The temperature at which it is possible to apply these alloys ranges from the liquid helium temperature (-269°C) to 540–815°C. At such temperatures, the superalloys can be used in conventional and nuclear power generation, aviation technology, chemical and petrochemical industries, electromachinery industry, cryogenics, and the manufacture of tools for the processing of non-ferrous metals and alloys.

Fe-Ni alloys are widely applied for operation at elevated and high temperatures, where they can be used as a structural material intermediate between types of martensitic steel used for operation at temperatures up to 600°C, and types of creep-resistant nickel superalloys intended for operation at temperatures above 700°C. Creep-resistant Fe-Ni alloys precipitation strengthened, compared to Ni- and Co-based alloys, have lower resistance to oxidation and gas corrosion, but have a high creep resistance at an intermediate range of temperatures, i.e. 540÷700°C. It may be expected that along with the continuous intensification of technological processes, increases in the operating parameters of machines in the energy generation industry, and the development of new technologies in the chemical, petrochemical, and processing industries, this group of materials will gain a more important role. The analysis of the current state of research on Fe-Ni alloys precipitation strengthened demonstrated that they are an interesting scientific problem, but also have utilitarian aspects, as their cost of manufacture is considerably lower in comparison to nickel and cobalt superalloys.

Alloys strengthened by precipitated ordered intermetallic phase γ' - $Ni_3(Al,Ti)$ with a regular structure fcc are the main group of creep-resistant Fe-Ni superalloys. The γ' phase in Fe-Ni alloys precipitates in the form of spheroid, highly dispersed particles coherent with the γ solid solution. In many reports [1–5], the γ' phase was considered to be the major phase strengthening iron-based alloys. In high-temperature applications, particles of the γ' phase strengthen Fe-Ni alloys up to 750°C. At higher temperatures, the γ' phase transforms into the η - Ni_3Ti phase, with a hexagonal structure and lamellar morphology. In Fe-Ni alloys, the strengthening effect caused by the precipitation of the η phase is less pronounced in comparison to strengthening by the γ' phase. Reduction in the nickel content in the matrix caused by the precipitation of γ' and η phases, at the simultaneous presence of molybdenum or wolfram as additives strengthening the solid solution, creates conditions for the precipitation of particles from TCP phases - σ, Laves, G, χ, and μ, decreasing the plasticity of alloy. At the same time, the precipitation of carbides (MC, $M_{23}C_6$, and M_6C) and borides or carboborides of different morphology can occur. The structural stability of Fe-Ni alloys improves as a result of the partial replacement of iron by nickel. This process allows for the increase in the concentration of components strengthening the solid solution γ and improves creep resistance, without the formation of undesirable TCP-phases.

Knowledge of the kinetics of the precipitation process of secondary phases in Fe-Ni alloys during heat treatment and/or service is necessary to forecast their functional properties and microstructural stability in operating conditions. Previous studies [3–6] and the results of the author's own research [7, 8] on Fe-Ni alloys were mainly focused on the analysis of the precipitation of intermetallic phases (γ', η, and G) and carbides ($M_{23}C_6$, M_6C, and MC) during

heat treatment or service, and their effects on strength and plastic properties. However, there has been no comprehensive quantitative characterization prepared so far regarding changes in the diameter of γ' phase particles at elevated and high temperatures.

In the present study, research has been undertaken on the influence of prolonged aging on the course of precipitation and coagulation of γ' - $Ni_3(Al,Ti)$ phase in a high-temperature, creep-resisting Fe-Ni superalloy. The basic stereological parameters of the γ' phase particles have been determined and the growth step of the γ' phase has been analyzed on the basis of the LSW theory. It is assumed that the obtained test results will be used for forecasting the structural stability of the superalloy under the conditions of heat treatment and operation.

2. General Characteristic of Fe-Ni Superalloys

2.1. Basic groups of wrought Fe-Ni superalloys

Developmental work on creep-resistant wrought Fe-Ni alloys has been carried out in parallel with work on nickel superalloys. There are significant differences in physical, chemical, and mechanical properties between iron and nickel superalloys, caused mainly by differences in their chemical compositions. Nickel superalloys were created and developed through the chemical modification of nickel-chromium alloy (NiCr20), while Fe-Ni alloys were developed by modifying the chemical and phase composition of austenitic steel 18–8. Currently, many researchers [1, 2, 9, 10] claim that most creep-resistant Fe-Ni superalloys contain min. 36% Fe, max. 45% Ni and min. 12% Cr. However, the above contents of elements are not strictly followed. Recent research has led to the development of more than 20 types of iron alloys with complicated chemical compositions. Their original classification, based on the main mechanism of strengthening, chemical, and phase composition and development of Fe-Ni alloys is proposed in Table 1.

Analysis of the current state of research demonstrated that the group of creep-resistant wrought Fe-Ni superalloys includes a large number of materials diversified in terms of chemical composition, strengthening mechanism, obtained properties, and applications. The primary group of Fe-Ni superalloys includes materials strengthened by the precipitation of ordered intermetallic phases γ' - $Ni_3(Al,Ti)$ and/or γ'' - Ni_3Nb intended for work at temperatures from 540°C to 815°C. At temperature above 815°C, the precipitates of intermetallic phases γ' and γ'' become unstable and age into the equilibrium phases η - Ni_3Ti and δ - Ni_3Nb, which is associated with a significant decrease in their creep resistance. For this reason, at the upper range of working temperatures (900°C to 1100°C) Fe-Ni solid-solution strengthened alloys or ODS superalloys are mainly used. Both types of alloys can be hardened to achieve the parameters of precipitation-strengthened alloys. Values of the 1000-h stress-rupture for selected wrought Fe-Ni alloys are presented in Figure 1. The creep resistance of Fe-Ni super-alloys mainly depends on the concentration of nickel and iron, and the content of elements that produce solid-solution or precipitation hardening of the alloy.

No.	Alloy	Nominal composition [wt. %]													
		C	Mn	Si	Cr	Ni	Fe	Co	Mo	W	Nb	Ti	Al	B	Other
		Group I. Fe-Ni alloys of solid-solution strengthened													
1.	19-9DL	0.30	1.1	0.6	19.0	9.0	66.8	–	1.25	1.25	0.4	0.3	–	–	–
2.	17-14CuMo	0.12	0.75	0.5	16.0	14.0	62.4	–	2.5	–	0.4	0.3	–	–	3.0Cu
3.	16-25-6	0.06	1.35	0.7	16.0	25.0	50.7	–	6.0	–	–	–	–	–	0.15N
4.	Incoloy 800	0.05	0.8	0.5	21.0	32.5	45.7	–	–	–	–	0.4	0.4	–	0.4Cu
5.	Incoloy 801	0.05	0.8	0.5	20.5	32.0	46.3	–	–	–	–	1.1	–	–	0.2Cu
6.	Incoloy 802	0.35	0.8	0.4	21.0	32.5	44.8	–	–	–	–	0.8	0.6	–	0.4Cu
7.	Carpenter 20Cb-3	0.07	0.8	0.4	20.0	34.0	42.4	–	2.5	–	1.0	–	–	–	3.5Cu
		Group II. Fe-Ni alloys of precipitation strengthened by γ' phase													
8.	W-545	0.08	1.5	0.4	13.5	26.0	55.8	–	1.5	–	–	2.85	0.2	0.080	–
9.	A-286	0.05	1.4	0.4	15.0	26.0	55.2	–	1.25	–	–	2.0	0.2	0.003	0.3V
10.	Discaloy	0.04	0.9	0.8	13.5	26.0	55.0	–	2.75	–	–	1.75	0.25	–	–
11.	Tinidur	0.04	1.0	0.75	14.5	26.0	54.0	–	1.25	–	–	2.15	0.2	0.003	0.03V
12.	V-57	0.08	0.35	0.75	14.8	27.0	48.6	–	1.25	–	–	3.0	0.25	0.010	0.5V
		Group III. Fe-Ni alloys with low thermal expansion													
13.	Incoloy 903	0.04			0.1	38.0	41.0	15.0	0.1	–	3.0	1.4	0.7	–	–
14.	Incoloy 907	0.01	0.3	0.15	0.1	38.0	42.0	13.0	–	–	4.7	1.5	0.03	–	–
15.	Incoloy 909	0.01		0.4	0.1	38.0	42.0	13.0	–	–	4.7	1.5	–	0.001	–
16.	Pyromet CTX-1	0.03			0.1	37.0	39.0	16.0	0.1	–	3.0	1.7	1.0	–	–
17.	Pyromet CTX-3	0.05	–	0.15	0.2	38.0	41.0	13.5	–	–	4.9	1.6	0.1	0.007	–
		Group IV. Fe-Ni and Ni-Fe alloys of precipitation strengthened by γ' and/or γ'' phases													
18.	CG27	0.05	0.1	0.1	13.0	38.0	38.4	–	5.7	–	0.7	2.5	1.6	0.010	–
19.	Incoloy 901	0.05	0.1	0.1	12.5	42.5	36.0	–	5.7	–	–	2.8	0.2	0.015	–
20.	Pyromet 860	0.05	0.05	0.05	12.6	43.0	30.0	4.0	6.0	–	–	3.0	1.25	0.010	–
21.	D-979	0.05	0.3	0.2	15.0	45.0	27.0	–	4.0	–	–	3.0	1.0	0.010	–
22.	Incoloy 706	0.03	0.2	0.2	16.0	41.5	40.0	–	–	–	2.9	1.8	0.2	–	–
23.	Inconel 718	0.04	0.2	0.2	19.0	52.5	18.5	–	3.0	–	5.1	0.9	0.5	–	–
		Group V. Fe-Ni and Ni-Fe alloys of precipitation strengthened by carbides													
24.	N-155	0.10	1.5	0.5	21.0	20.0	32.2	20.0	3.0	2.5	1.0	–	–	–	0.15N; ≤0.5Cu
25.	Haynes 556	0.10	1.5	0.4	22.0	20.0	29.0	20.0	3.0	2.5	0.1	–	0.3	–	0.5Ta; 0.02La; 0.002Zr

No.	Alloy	Nominal composition [wt. %]													
		C	Mn	Si	Cr	Ni	Fe	Co	Mo	W	Nb	Ti	Al	B	Other
		Group I. Fe-Ni alloys of solid-solution strengthened													
26.	Hastelloy X	0.10	0.5	0.5	22.0	47.0	18.5	1.5	9.0	0.6	–	–	–	–	–
		Group VI. Fe-Cr alloys of oxide dispersion strengthened (ODS)													
27.	Incoloy MA956	0.05			20.0		74.4					0.5	4.5		$0.5Y_2O_3$
28.	Incoloy MA957	0.05			14.0		84.4		0.3			1.0			$0.25Y_2O_3$
29.	PM2000 Alloy	0.05			20.0		73.4					0.5	5.5		$0.5Y_2O_3$

Table 1. Nominal chemical composition of selected wrought Fe-Ni, Ni-Fe, and Fe-Cr superalloys [11, 12].
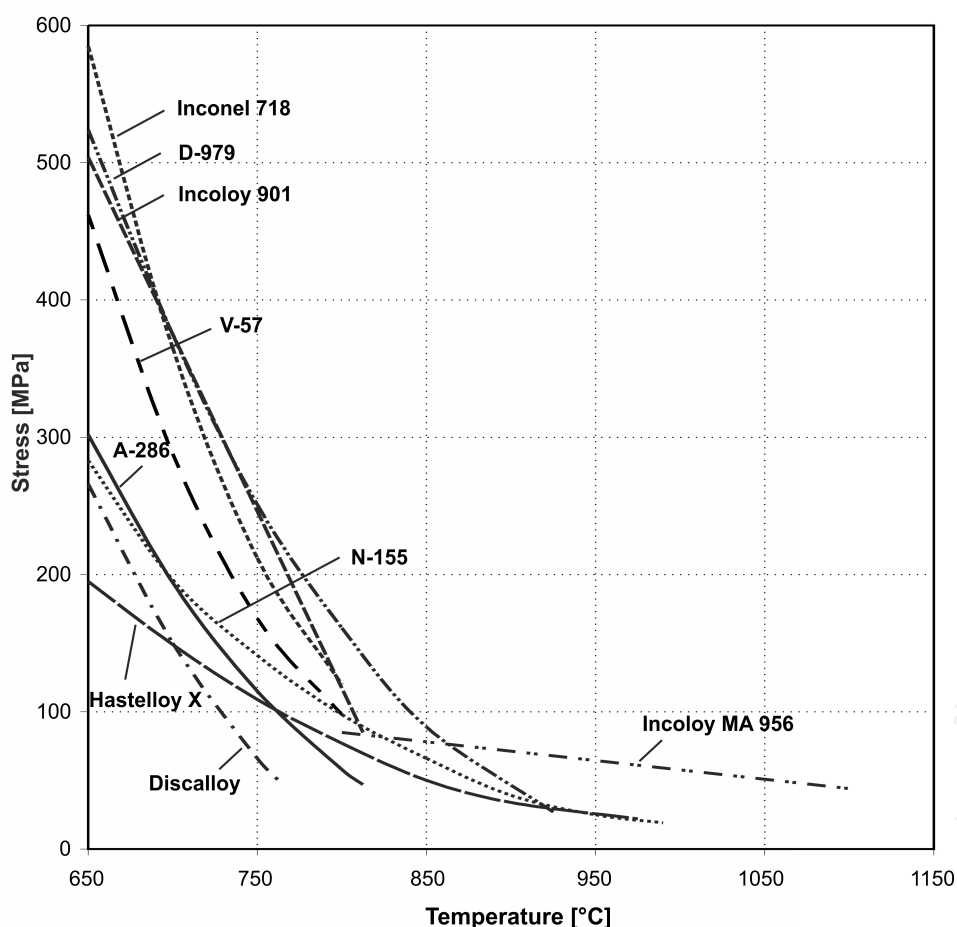
Figure 1. h stress-rupture curves of wrought superalloys of Fe-Ni, Ni-Fe and Fe-Cr type [2].

The increased content of nickel in Fe-Ni alloys is usually associated with good creep resistance, higher working temperatures, better thermal stability of microstructure, and higher price.

On the other hand, high iron content, despite reduced cost and improved machinability of the material, increases the melting point and decreases the resistance of the alloy to oxidation.

Creep-resistant Fe-Ni alloys, compared to nickel- and cobalt-based superalloys, have lower resistance to oxidation and gas corrosion, but have a high creep resistance at an intermediate range of temperatures, i.e. 540÷750°C.

Currently, novel types of ferritic ODS superalloys are strong competition for nickel and cobalt superalloys. They are popular due to their significantly lower price and good creep resistance (up to 1200°C). Fe-Ni superalloys, because of the similar phase composition, are frequently classified to the same group of materials as nickel superalloys [1, 2, 9]. Therefore, their further development is closely connected with the development of wrought creep-resistant nickel superalloys.

2.2. Elements interaction in Fe-Ni superalloys

High-temperature Fe-Ni superalloys are characterized by a complex chemical composition. There are as many as 15 significant elements, in the case of which control of their content enables solution strengthening and, at the same time, precipitation strengthening of the matrix and grain boundaries. Alloying elements can be divided into five principal groups, depending on their effect in the shaping of the microstructure and properties (Figure 2):

- matrix-strengthening elements: Fe, Ni, Co, Cr, Mo, W, and V;

- elements forming γ'- type intermetallic phases: $Ni_3(Al,Ti)$ and γ'' - Ni_3Nb – Al, Ti, Nb, and Ta;

- elements that enhance oxidation resistance: Cr, Al, and La;

- elements that effect grain boundaries: B, C, Zr, and Hf;

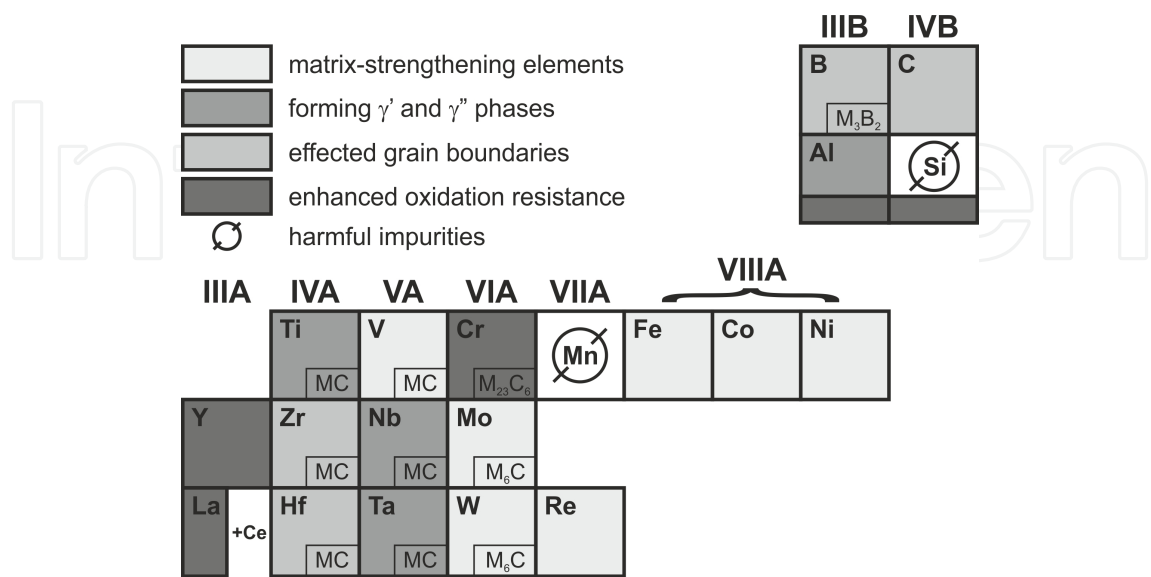- harmful impurities: Si and Mn.

Figure 2. Interaction of alloying elements in iron- and nickel-base superalloys [1, 13].

Some elements, numbered among carbide-forming ones, form carbides and carbonitrides in the alloy, as well as borides and carboborides. The first group of alloying components, introduced mostly to strengthening the solid solution γ, includes most often [1, 2, 9, 10, 13]: Cr (12÷22%), Mo (up to 6%), W (up to 3%), and Co (up to 20%). The second group of elements introduced in order to form γ'- type intermetallic phases such as $Ni_3(Al,Ti)$, and/or γ''- type phases such as Ni_3Nb, and to induce precipitation strengthening includes Ti (up to 3%), Al (up to 1.2%), Nb (up to 5%), and sometimes Ta (up to 0.5%). The third group of alloy additions, whose purpose is to enhance oxidation resistance at high temperatures are: Cr (12÷22%) and aluminium (up to 5.5%). The fourth group, i.e., the elements added in order to improve the ductility of grain boundaries and creep resistance, includes micro-additions of B (up to 0.015%), Zr (up to 0.002%), and V (up to 0.5%) [1, 2, 13, 14]. Micro-additions of boron and zirconium segregate to the grain boundaries, reduce the energy of their mismatch, and influence the morphology of carbides and intermetallic phases. A vanadium addition improves resistance to notch effect at elevated temperatures and hot deformability of alloys. Deformability of alloys can be also increased by small contents, from 0.01% to 0.05%, of magnesium or rare-earth metals (REM). These elements also counteract brittleness caused by sulfur [1, 2, 6, 13, 21]. New generation iron superalloys contain elements from the lanthanide and actinide groups (e.g., La, Th, and Y), which improve alloys' resistance to high-temperature oxidation [2, 10, 15]. In the group of wrought superalloys, ODS alloys have been gaining importance over the latest period, as well as alloys produced by powder metallurgy methods (P/M) [2, 13, 15–19]. A detailed breakdown of the interaction of the main alloying elements in iron and nickel superalloys is presented in Table 2.

Effect	Iron-based superalloys	Nickel-based superalloys
Solid-solution strengtheners	Cr, Mo, W, Co	Co, Cr, Fe, Mo, W, Ta
Fcc matrix stabilizers	C, W, Ni	---
Carbide form:		
MC type	Ti	W, Ta, Ti, Mo, Nb
M_7C_3 type	---	Cr
M23C6 type	Cr	Cr, Mo, W
M6C type	Mo	Mo, W
Carbonitrides		
– M(C,N)	C, N	C, N
Forms γ' - $Ni_3(Al,Ti)$	Al, Ni, Ti	Al, Ti
Retards formation of hexagonal η - Ni_3Ti	Al, Zr	---
Raises solvus temperature of γ'	---	Co
Hardening precipitates and/or intermetallics	Al, Ti, Nb	Al, Ti, Nb, Ta
Forms γ'' - Ni_3Nb	Nb	Nb

Effect	Iron-based superalloys	Nickel-based superalloys
Oxidation resistance	Cr, Al	Cr, Al, Ta
Improves hot corrosion resistance	La, Y	La, Th
Sulfidation resistance	Cr	Cr
Increases rupture ductility	B[1], Zr	B[1], Zr
Causes grain-boundary segregation	---	Mg, B, C, Zr
Facilitates working	V	---

[1] If present in large amount, borides are formed

Table 2. Role of elements in iron- and nickel-based superalloys [2, 13].

Silicon, phosphorus, sulfur, oxygen, and nitrogen are harmful in iron and nickel superalloys. First of all, they reduce the alloys' ductility during creep [1, 2, 13, 20, 21]. The content of these elements is limited and controlled by using relevant melting technologies. Also other trace elements, such as selenium, bismuth, lead, zinc, and arsenic should be kept at a low level (in the order of ppm). The content of harmful elements in iron and nickel superalloys is reduced by applying special vacuum metallurgy processes [13, 14, 22, 23]. Vacuum melting and casting prevent oxidation of the alloy, and allows better control over the principal, reactive elements. These processes also prevent an increase of the nitrogen content in the alloy during melting. As a result, the content of Al, Ti, and Nb is considerably increased through vacuum melting. In consequence, the relative volume of phase γ' and/or γ'' increases as well. However, the range of plastic working temperature of superalloys with a high content of Al, Ti, and Nb is narrow and close to the solidus line.

2.3. The basic phases in Fe-Ni superalloys and precipitation reactions

Creep-resisting Fe-Ni superalloys are basically Fe-Ni-Cr alloys with a number of added elements that form substitutional and interstitial solid solutions, and are introduced in order to ensure solution and precipitation strengthening of the matrix. Equilibrium phases in Fe-Ni alloys depend mostly on the content of three basic elements, i.e., Fe, Cr, and Ni (Figure 3). The analysis of the phase composition at a temperature of 1,050°C and 650°C shows that the Fe-Ni alloys with a content of ca. 13÷22% Cr, ca. 15÷42% Ni, and ca. 36÷60% Fe, have a structure of a disordered solid solution γ with a regular fcc structure.

In γ solid solutions, in the case of a majority of creep-resisting Fe-Ni superalloys, efforts are made to ensure an appropriate proportion of iron and nickel contents. The value of this proportion determines the thermal stability of the alloy microstructure, its operation temperature, and cost. An increased nickel content in Fe-Ni alloys usually allows increasing the concentration of elements strengthening the solid solution without the formation of undesirable TCP or other phases [1–3, 5]. Therefore, alloys with a high nickel content are characterized by good structural stability and creep resistance, which enables their use at high operating
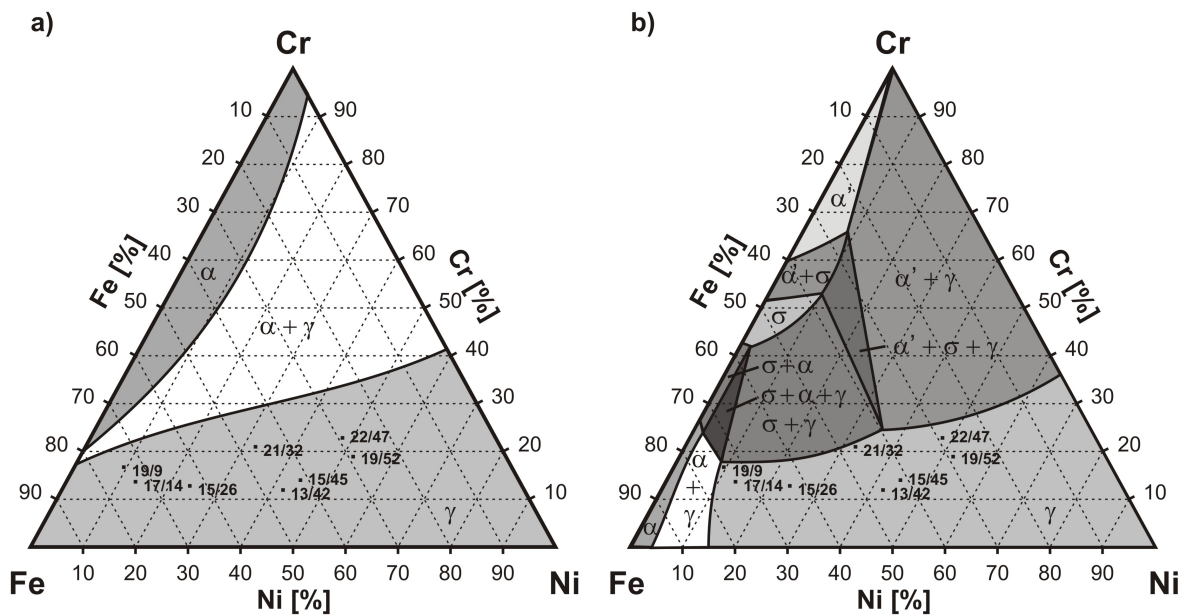
Figure 3. Cross-sections of isothermal phase diagram of Fe-Cr-Ni at a temperature [24]: a) 1,050°C; b) 650°C.

temperatures. The minimum nickel content that is necessary to form a stable γ solid solution in a majority of Fe-Ni alloys amounts to ca. 25% [1, 5, 14]. A cobalt additive or other additives stabilizing the γ phase allow reducing the required nickel level. At the same time, an increased iron content affects adversely on heat resistance. Iron oxides feature poor adhesion to the substrate. An increased iron content also enhances the susceptibility of Fe-Ni alloys to precipitation of the disadvantageous TCP phases, including in particular the σ phase.

The introduction of alloying elements to Fe-Ni alloys results in the formation in the γ solid solution of numerous precipitates of intermetallic phases, carbides, carbonitrides, borides, and carboborides, which do not always have a good effect on the properties of the alloys. Knowledge of the kinetics of the precipitation process of secondary phases in Fe-Ni alloys during heat treatment and/or service is necessary to forecast the changes in the characteristics of their mechanical, physical, and chemical properties. The issue of precipitation processes in creep-resisting Fe-Ni superalloys is addressed in a number of papers. The most important ones are those by Stickler [3], Dulis [4], Pickering [5], Sourmail [6], and the author's own studies [7,8,11]. Based on the research results obtained, it was found that a number of stable and metastable phase components, similar to those observed in nickel superalloys, are present in the microstructure of Fe-Ni alloys (Table 3). It should be pointed out that due to considerable differences in the chemical compositions of superalloys and their manufacturing technologies, the phases of the same type present in them may show significant differences in the chemical compositions and morphologies.

After heat treatment Fe-Ni superalloys consist of a matrix of a strengthened solid solution, γ, with dispersion particles of GCP intermetallic phases (mostly γ' and/or γ''), carbide precipitates (MC, M_6C, $M_{23}C_6$, M_7C_3) and, possibly, precipitates of nitrides, carbonitrides, borides, and carboborides [2,3,4,5,6,13].

Phases	Iron-based superalloys	Nickel-based superalloys
Matrix	γ – gamma, nonordered fcc, (Fe, Ni, Cr, ...).	γ – gamma, non ordered fcc, (Ni, Cr, Co, ...).
Geometrically close-packed (GCP)	γ' – gamma prime, ordered fcc, AB_3 type, (Ni, ...)$_3$(Al, Ti); γ''– gamma double prime, ordered bct, AB_3 type, Ni_3Nb; η – eta, hcp, AB_3 type, Ni_3Ti; δ – delta, orthorombic, AB_3 type, Ni_3Nb; β – beta, bcc, AB type, NiAl.	γ' – gamma prime, ordered fcc, AB_3 type, (Ni, Co, Fe, Cr, ...)$_3$(Al, Ti); γ''– gamma double prime, ordered bct, AB_3 type, Ni_3Nb; η – eta, hcp, AB_3 type, Ni_3Ti; δ – delta, orthorhombic, AB_3 type, Ni_3Nb.
Topologically close-packed (TCP)	σ – sigma, bct, AB type, Fe-Ni-Cr-Mo; Laves – hcp, A_2B type, Fe_2Mo, Fe_2W, Fe_2(Ti, Nb); G – fcc, $A_{16}D_6C_7$ type, $Ni_{16}Ti_6Si_7$, $Ni_{16}Nb_6Si_7$; μ – mu, rhombohedral, A_6B_7 type, (Cr, W)$_6$(Fe, Co)$_7$; χ – chi, bcc, (Fe, Cr, Mo) or $M_{18}C$ type, $Fe_{36}Cr_{12}Mo_{10}$.	σ – sigma, bct, A_xB_y type, (Fe, Mo)$_x$(Ni, Co)$_y$; Laves – hcp, A_2B type, (Fe, Cr, Mn, Si)$_2$(Mo, Ti, Nb); G – fcc, A_6B_{23} type, $Hf_6Ni_8Al_{15}$; μ – mu, rhombohedral, A_6B_7 type, (Mo, W)$_6$(Ni, Co)$_7$.
Carbides	MC – fcc, (Ti, Nb, V, Zr, Ta)C; M_7C_3 – trigonal, Cr_7C_3; $M_{23}C_6$ – fcc, (Cr, Ni, Mo, Fe)$_{23}C_6$; M_6C – diamond type fcc, (Fe, Cr)$_{21}Mo_3C$, Fe_3Nb_3C.	MC – fcc, (Ti, Mo, Nb, Ta, W)C; M_7C_3 – trigonal, Cr_7C_3; $M_{23}C_6$ – fcc, (Cr, Mo, Co, W, Nb)$_{23}C_6$; M_6C – diamond type fcc, (Ni, Co)$_3Mo_3C$, (Ni, Co)$_2W_4C$.
Borides and carboborides	$M_{23}(C,B)_6$ – fcc,	M_3B_2 – tetragonal, (Mo, Ti, Cr, Ni, Co)$_3B_2$; $M_{23}(C,B)_6$ – fcc.
Nitrides and carbonitrides	MX – fcc, Ti(C, N), Nb(C, N); MN_2 – hcp, Cr_2N.	MX – fcc, Ti(C, N); $M_{23}(C, N)_6$ – fcc.

Phases		Iron-based superalloys	Nickel-based superalloys
Others	$M(C, N, P)$;		$Ni_x(Mo, Cr)_y(C, Si)$;
	$(M, P)_{23}C_6$;		$Ti_4C_2S_2$;
	Cr_3Ni_2Si;		ZrS_x.
	α' – alpha prim, bcc,		
	(Cr, Fe);		
	$Ti_4C_2S_2$.		

Table 3. Phases identified in iron- and nickel-base superalloys [2, 3, 6, 13].

Such a microstructure is stable in a narrow range of temperature and time parameters, and may be unsuitable for the operating conditions. The effect of such instability is the changes in the chemical composition, morphology, arrangement, and properties of the phases present in complex temperature, stress, and environment-related conditions. The undesirable phases may develop during heat treatment or thermo-mechanical exposure, depending on the reactions between the different phases that are affected by the segregation of alloying and trace elements, as well as the interaction with crystallographic defects. The sequence of the precipitation reactions taking place in iron and nickel superalloys is the effect of changes in the chemical composition of the matrix that occur during heat treatment, and the thermo-mechanical interactions that occur in service. Table 4 summarizes the most important precipitation reactions proceeding in iron- and nickel-based superalloys during heat treatment and during operation at elevated temperatures.

No.	Iron-based superalloys	No.	Nickel-based superalloys
A.	During initial heat treatment:	A.	During initial heat treatment:
1.	$\gamma \rightarrow$ GCP $(\gamma', \gamma'', \eta, ...) + \gamma^*$	1.	$\gamma \rightarrow \gamma' + \gamma^*$
2.	$\gamma \rightarrow M_xC$ (MC, $M_{23}C_6$, ...) $+ \gamma^*$	2.	$\gamma \rightarrow M_xC$ (MC, $M_{23}C_6$, M_6C, ...) $+ \gamma^*$
B.	During extended exposure to elevated temperatures:	B.	During extended exposure to elevated temperatures:
		1.	$\gamma^* \rightarrow$ TCP $(\sigma, Lavesa, ...)$
1.	$\gamma^* \rightarrow$ TCP $(G, \sigma, \chi, Lavesa, ...)$	2.	$\gamma^* + MC \rightarrow \gamma' + \gamma^{**}$ ("/> 900°C)
2.	$\gamma' \rightarrow \eta$	3.	$\gamma^* + MC \rightarrow \gamma' + M_{23}C_6$
3.	$\gamma'' \rightarrow \delta$	4.	$\gamma^* + MC \rightarrow \gamma' + M_6C$
4.	$\gamma' \rightarrow \beta$	5.	$\gamma^* + M_6C \rightarrow M_{23}C_6 + \gamma^{**}$
5.	$M_{23}C_6 \rightarrow$ TCP $+ \gamma^{**}$ (C in solution)	6.	$\gamma' \rightarrow \eta$
		7.	$MC + M \rightarrow M_7C_3 + M \rightarrow M_{23}C_6 + TCP(\sigma)$

Where: γ^* – gamma phase depleted in certain alloying elements;

γ^{**} – gamma phase of slightly different composition

Table 4. The basic phase reactions proceeding in iron- and nickel-based superalloys [3, 5, 13].

When comparing creep-resisting iron and nickel superalloys, it can be noted that with an increasing iron content in Fe-Ni alloys, the following disadvantageous interactions appear [1, 2, 3, 13, 25]:

- the dissolution temperature of the main strengthening phases, γ' and γ'', decreases;

- susceptibility to overaging and precipitation of the η and δ phases increases;

- susceptibility to the formation of TCP – σ, Laves, G, χ, and μ phases also increases;

- the mismatch parameters of the γ/γ' and γ/γ'' lattice change because iron, compared to nickel, has a greater (by ca. 3%) atomic diameter.

It can be concluded that the final effect of these adverse interactions is the much lower operating temperature (815°C) of Fe-Ni alloys in creep-resisting applications compared to the maximum operating temperature (1,090°C) of wrought nickel superalloys.

3. Material and methodology

The examinations were performed on rolled bars, 16 mm in diameter, of an Fe-Ni superalloy of the A-286 type. The chemical composition of the material is given in Table 5.

Content of an element [wt. %]															
C	Si	Mn	P	S	Cr	Ni	Mo	V	W	Ti	Al	Co	B	N	Fe
0.05	0.56	1.25	0.026	0.016	14.3	24.5	1.35	0.42	0.10	1.88	0.16	0.08	0.007	0.0062	55.3

Table 5. Chemical composition of the investigated Fe-Ni superalloy.

Test specimens cut from the bars underwent solution heat treatment at 980°C for 2 h followed by water quenching. Next, they were aged at 715°C, 750°C and 780ºC, with the holding time ranging between 0.5 h and 500 h (Figure 4). The aging temperature (in the range of 715–780°C) and time (up to 500 h) were selected based on the possibility of simulating the operation of the alloy for 100,000 h at temperatures of 630–690°C, according to the Larson-Miller parameter [26].

Examination of the structure was performed with a Jeol JEM-200 FX transmission electron microscope by means of the thin foil technique. A Philips PW-140 X-ray diffractometer was used for the phase analysis of the isolates that formed during anodic dissolution of the specimens in a 10% hydrochloric acid solution in ethanol, where the density of current amounted to 10–12 mA/cm².

Quantitative analysis of the secondary phase particles, γ' - $Ni_3(Al,Ti)$, was performed on thin foil images (TEM) in the bright field. Images of the microstructure (TEM) were transformed into binary images using the computer program Met-Ilo [27]. On their basis, the basic stereological parameters of the γ' phase were determined: the mean diameter of particles on the
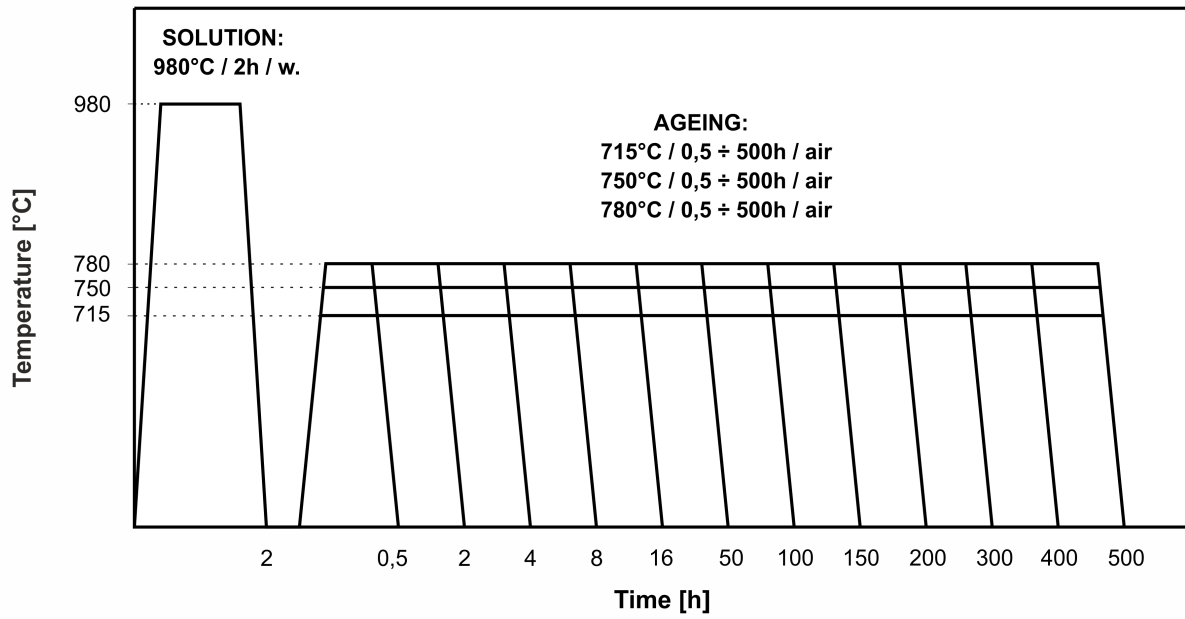
Figure 4. Scheme of heat treatment of the investigated Fe-Ni superalloy.

circles in the projected plane $\bar{d}$, the mean diameter of particles $\overline{D}$, the volume fraction of particles V_V, and the mean distance between particles, l_d.

The mean diameter of particles $\bar{d}$ on the circles in the projected plane of phase γ' was determined from the equation [28]:

$$\bar{d} = \sqrt{\frac{4A'}{\pi}} \tag{1}$$

where: A' – particles surface on the circles (on image TEM) [nm^2].

The mean diameter $\overline{D}$ of the particles was evaluated with help of the relation given by Czyrska-Filemonowicz et al. [29]:

$$\overline{D} = \frac{\bar{d}t}{t - \bar{d} + \left(\pi A_A / L_A\right)} \tag{2}$$

.

where: t – the foil thickness [nm], A_A – the projection area, L_A – the perimeter density [1/nm].

The volume fraction V_V of γ' particles was calculated using the formula provided by Dubiel et al. [30]:

$$V_V = \frac{\pi}{6} \frac{\sum N_i d_i^3}{A\left(t + \bar{d}\right)} \tag{3}$$

where: N_i – number of particles with diameter d_i, A – total projection area [nm^2].

The mean distance between particles l_d was calculated by means of an equation given by Schröder and Arzt [31]:

$$l_d = \bar{d}\sqrt{\frac{\pi}{6V_V}\left(1 + \frac{s^2}{\bar{d}^2}\right)} - \frac{\pi}{4}\bar{d} \tag{4}$$

where: s – standard deviation of the particle diameter distribution.

4. Results and discussion

4.1. Precipitation processes in the Fe-Ni superalloy during prolonged aging

After a 2-hour solution heat treatment at the temperature of 980°C and water quenching, the structure of the Fe-Ni superalloy resembles twinned austenite with a small amount of undissolved precipitates (ca. 0.3 wt. %) and an elevated dislocation density (Figures 5 and 6). Presence of titanium compounds such as carbide TiC, carbonitride $TiC_{0.3}N_{0.7}$, nitride $TiN_{0.3}$, carbosulfide $Ti_4C_2S_2$ and Laves phase Ni_2Si and boride MoB were found in the extracted precipitates (Figure 7).
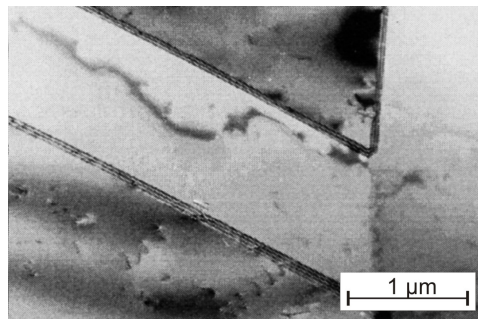
Figure 5. Alloy microstructure after solution heat treatment at 980°C/2 h/w. Twinned austenite with dislocations and undissolved carbosulfide $Ti_4C_2S_2$.
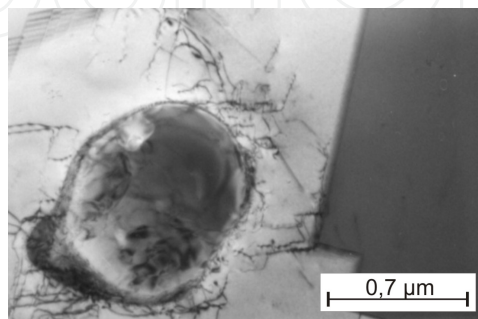
Figure 6. Alloy microstructure after solution heat treatment at 980°C/2 h/w. Twinned austenite with an increased dislocation density and undissolved carbide TiC.
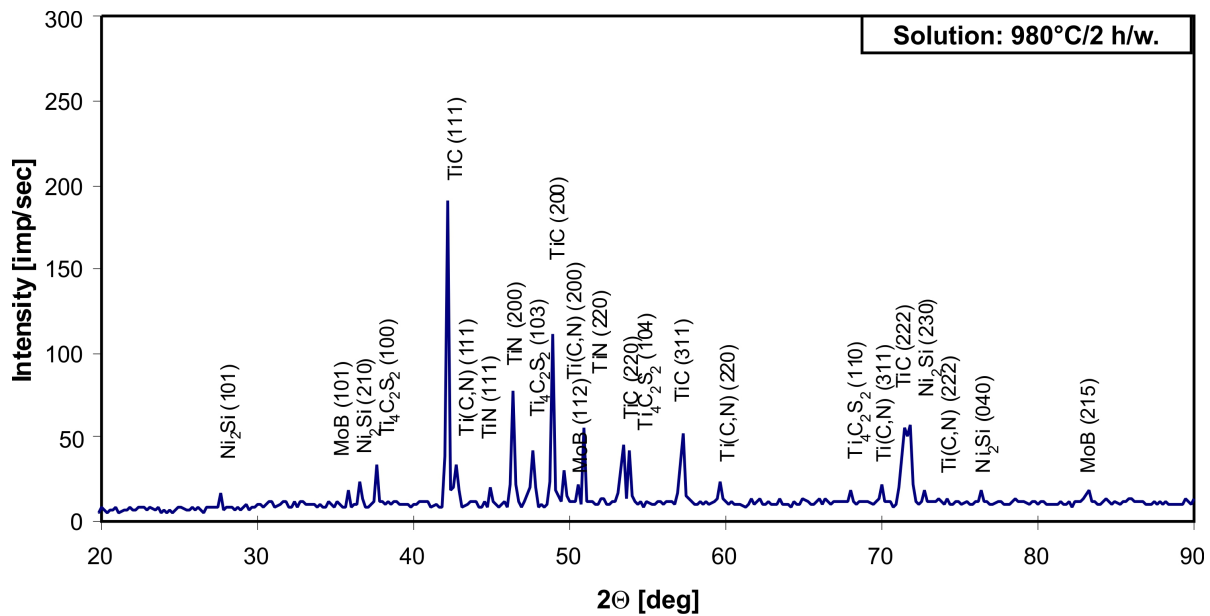
Figure 7. Isolate diffractogram of the alloy after solution heat treatment at 980°C/2 h/w.

One-stage aging applied after solution heat treatment at the above-specified temperatures of 715°C, 750°C, and 780°C in time between 0.5 h and 500 h causes initiation of precipitation and coagulation, as well as overaging of carbides and intermetallic phases. After short-period (4-8 h) aging at 715°C, effects of the initial precipitation phases can be observed in the matrix, including clusters of the γ' -Ni$_3$ (Al, Ti) phase and coherent zones (Figure 8). As Pickering [5] and Wilson [32] claim, this phenomenon is connected with spinodal decomposition of supersaturated austenite. In this way, areas rich in Ti and Al were formed homogenously in the matrix. Fine lenticular lamellae of phase G (Ni$_{16}$Ti$_6$Si$_7$) in the form of chains, characteristic of discontinuous precipitation, appeared on grain boundaries (Figure 9). In the case of extending the aging time (within a range of 16 h – 500 h), the kinetics increased the homogeneous precipitation of the γ' phase particles in the matrix (Figure 10). In addition, presence of lenticular carbide particles M$_{23}$C$_6$ was detected in the region near the austenite boundary (Figure 11). The presence of carbide TiC, carbonitride TiC$_{0.3}$N$_{0.7}$, nitride TiN$_{0.3}$, carbosulfide Ti$_4$C$_2$S$_2$ and MoB and M$_3$B$_2$ borides were also detected in the alloy microstructure (Figure 12, Table 6).
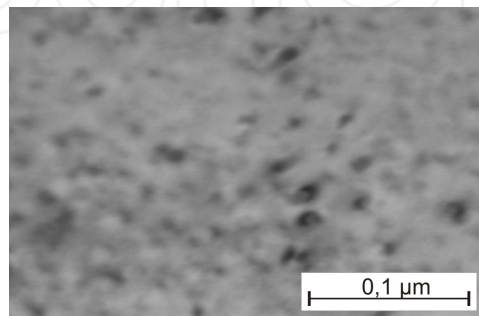

Figure 8. Alloy microstructure after solution heat treatment and aging at 715°C/4 h. Coherent zones and clusters of phase γ' in the austenite region.
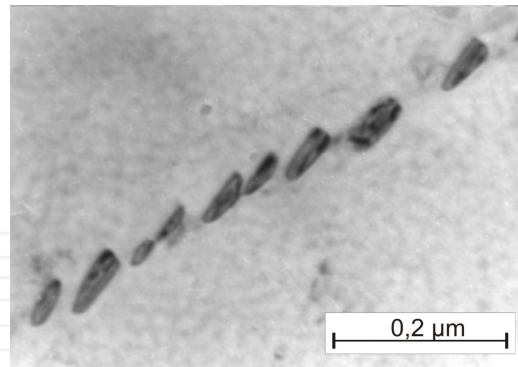
Figure 9. Alloy microstructure after solution heat treatment and aging at 715°C/8 h. Coherent zones of phase γ' in the matrix and lamellae of phase G on the grain boundary.
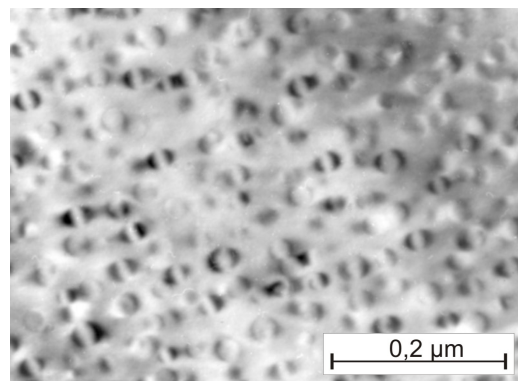

Figure 10. Alloy microstructure after solution heat treatment and aging at 715°C/150 h. Coherent spherical particles of phase γ' in the austenite.
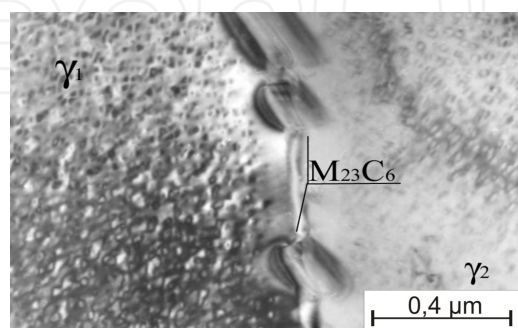

Figure 11. Alloy microstructure after solution heat treatment and aging at 715°C/300 h. Dispersive precipitates of phase γ' in the matrix and lenticular particles of $M_{23}C_6$ carbide on the grain boundary.
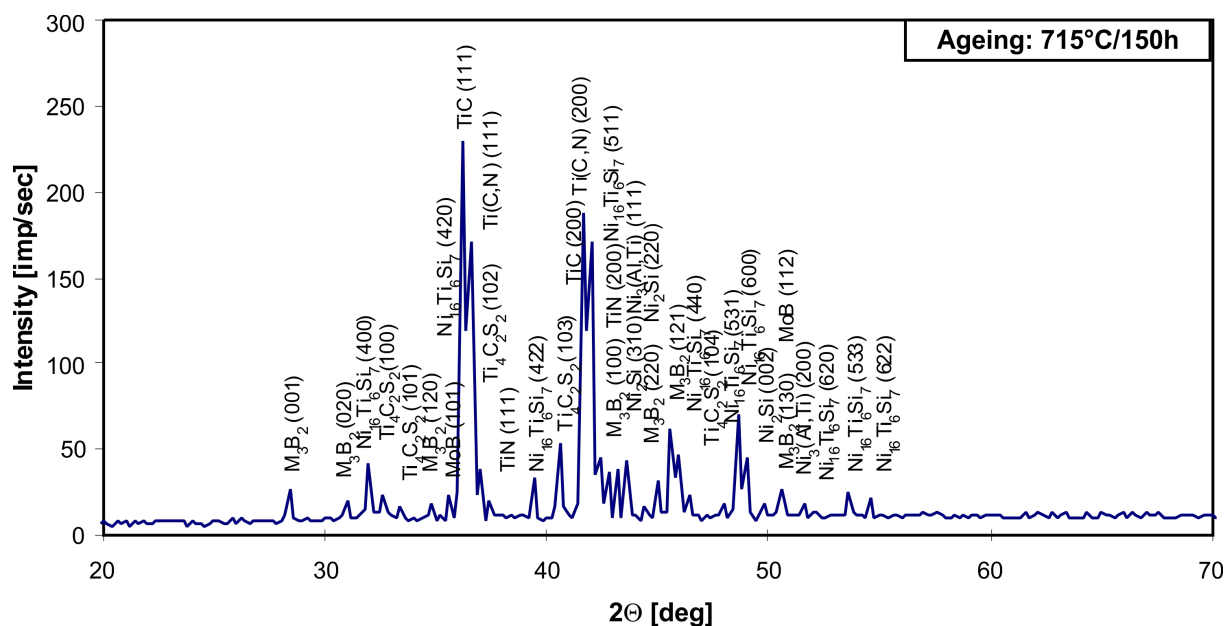
Figure 12. Isolate diffractogram of the alloy after solution heat treatment and aging at 715°C/150 h.

Alloy condition	Phase constituents
Solution heat treatment: 980°C/2 h/w	TiC; TiC$_{0,3}$N$_{0,7}$; TiN$_{0,3}$; Ti$_4$C$_2$S$_2$; Ni$_2$Si; MoB
Aging: 715°C/0.5 h	TiC; TiC$_{0,3}$N$_{0,7}$; TiN$_{0,3}$; Ti$_4$C$_2$S$_2$; Ni$_2$Si; MoB; G – Ni$_{16}$Ti$_6$Si$_7$
Aging: 715°C/2÷500 h	TiC; TiC$_{0,3}$N$_{0,7}$; TiN$_{0,3}$; Ti$_4$C$_2$S$_2$; Ni$_2$Si; MoB; G - Ni$_{16}$Ti$_6$Si$_7$; γ' - Ni$_3$(Al,Ti); M$_3$B$_2$

Table 6. Phase composition of the Fe-Ni alloy isolates after solution heat treatment and aging at 715°C.

An increase in the aging temperature of the alloy to 750°C leads to intensification of the diffusive processes of coagulation, growth, and overaging of intermetallic phase and carbide particles. Where aging time is extended (within a range of 16 h – 50 h), lenticular and spheroidal particles of phase γ' precipitate, showing strong coherence with the matrix (Figure 13). The first signs of overaging were found in the structure of the alloy after 100 h – 300 h, where colonies of transcrystalline Widmanstätten lamellae were formed. The lamellae of phase η (Ni$_3$Ti) grew into the austenite grain in the <111> direction (Figure 14). The phase transition γ' → η was accompanied with dissolution of fine particles of the neighboring γ' phase. In addition, presence of carbide TiC, carbonitride TiC$_{0.3}$N$_{0.7}$, nitride TiN$_{0.3}$, carbosulfide Ti$_4$C$_2$S$_2$, and particles of the Laves phase (Ni$_2$Si), phase G (Ni$_{16}$Ti$_6$Si$_7$), phase β (NiTi), phase σ (Cr$_{0.46}$Mo$_{0.40}$Si$_{0.14}$), and boride MoB were also detected in the alloy microstructure (Figure 15, Table 7).
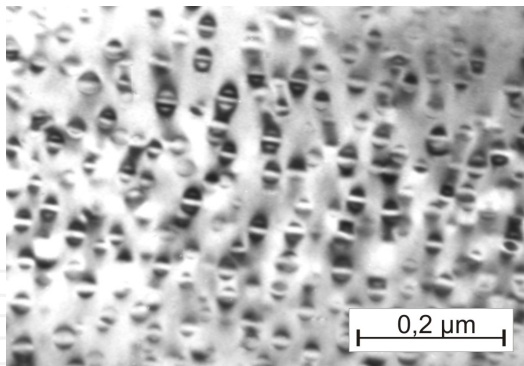
Figure 13. Alloy microstructure after solution heat treatment and aging at 750°C/50 h. Coherent spheroidal and lenticular particles of γ' in the matrix.
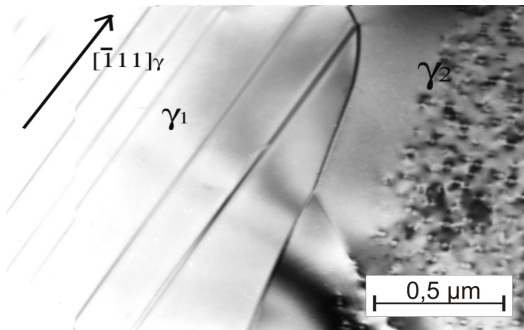

Figure 14. Alloy microstructure after solution heat treatment and aging at 750°C/100 h. Parallel lamellae of phase η in the matrix.
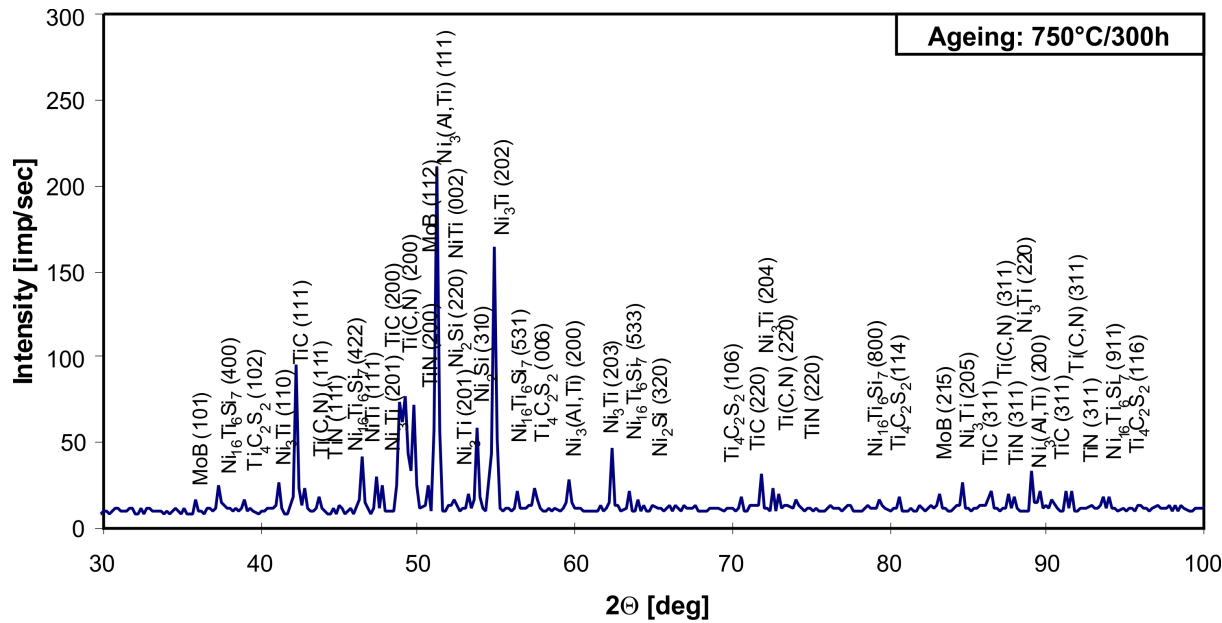

Figure 15. Isolate diffractogram of the alloy after solution heat treatment and aging at 750°C/300 h.

Alloy condition	Phase constituents
Solution heat treatment: 980°C/2 h/w	TiC; TiC$_{0,3}$N$_{0,7}$; TiN$_{0,3}$; Ti$_4$C$_2$S$_2$; Ni$_2$Si; MoB
Aging: 750°C/2÷50 h	TiC; TiC$_{0,3}$N$_{0,7}$; TiN$_{0,3}$; Ti$_4$C$_2$S$_2$; Ni$_2$Si; MoB; G - Ni$_{16}$Ti$_6$Si$_7$; γ' - Ni$_3$(Al,Ti)
Aging: 750°C/100÷150 h	TiC; TiC$_{0,3}$N$_{0,7}$; TiN$_{0,3}$; Ti$_4$C$_2$S$_2$; Ni$_2$Si; MoB G - Ni$_{16}$Ti$_6$Si$_7$; γ' - Ni$_3$(Al,Ti); η - Ni$_3$Ti
Aging: 750°C/200÷300 h	TiC; TiC$_{0,3}$N$_{0,7}$; TiN$_{0,3}$; Ti$_4$C$_2$S$_2$; Ni$_2$Si; MoB G - Ni$_{16}$Ti$_6$Si$_7$; γ' - Ni$_3$(Al,Ti); η - Ni$_3$Ti; β – NiTi
Aging: 750°C/400÷500 h	TiC; TiC$_{0,3}$N$_{0,7}$; TiN$_{0,3}$; Ti$_4$C$_2$S$_2$; Ni$_2$Si; MoB G - Ni$_{16}$Ti$_6$Si$_7$; γ' - Ni$_3$(Al,Ti); η - Ni$_3$Ti; β - NiTi; σ - Cr$_{0,46}$Mo$_{0,40}$Si$_{0,14}$

Table 7. Phase composition of the Fe-Ni alloy isolates after solution heat treatment and aging at 750°C.

An increase in the aging temperature of the alloy to 780°C leads to intensification of the diffusive processes, such as coagulation and overaging of intermetallic phase and carbide particles. Extended aging time (from 50 h to 150 h) contributes to coagulation of phase γ' particles. Clear signs of non-dilatational strain were detected, which was connected with the occurrence of internal stacking faults (SF) (Figure 16), the latter being the nucleation sites of the η phase lamellae. The mechanism of the $\gamma' \rightarrow \eta$ transition was proposed by Merrick and Nicholson [33] who described it through the appearance of SF in the γ' phase whose lattice constants were slightly greater to those of the matrix. Furthermore, lamellar precipitates of the η phase were detected near the boundary of the cellular system (Figure 17). In addition, analysis of the phase composition of the isolated precipitates confirmed the presence of carbide TiC, carbonitride TiC$_{0.3}$N$_{0.7}$, nitride TiN$_{0.3}$, carbosulfide Ti$_4$C$_2$S$_2$, and particles of the Laves phase (Ni$_2$Si), phase G (Ni$_{16}$Ti$_6$Si$_7$), phase σ (Cr$_{0.46}$Mo$_{0.40}$Si$_{0.14}$), and boride MoB in the alloy microstructure (Figure 18, Table 8).

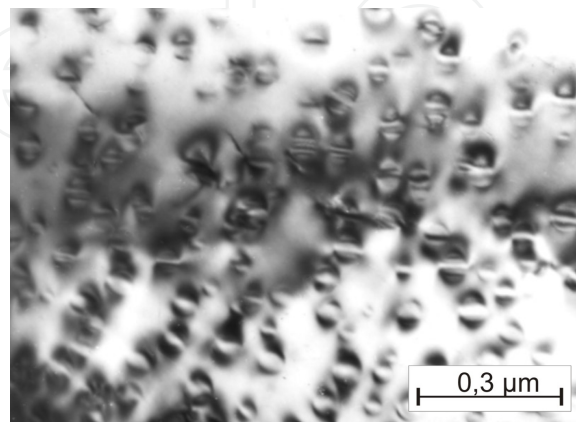**Figure 16.** Alloy microstructure after solution heat treatment and aging at 780°C/150 h. Nucleation of transcrystalline lamellae of phase η by means of the SF mechanism in phase γ'.
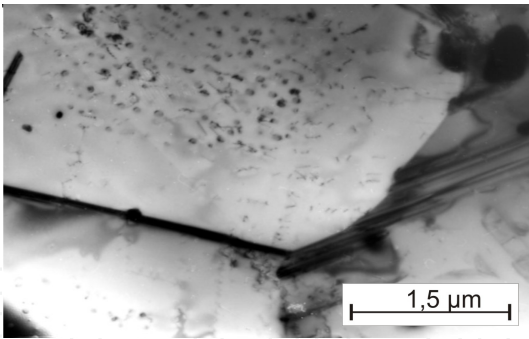
Figure 17. Alloy microstructure after solution heat treatment and aging at 780°C/500 h. Precipitates of lamellae η in the cellular system in the region near the boundary.
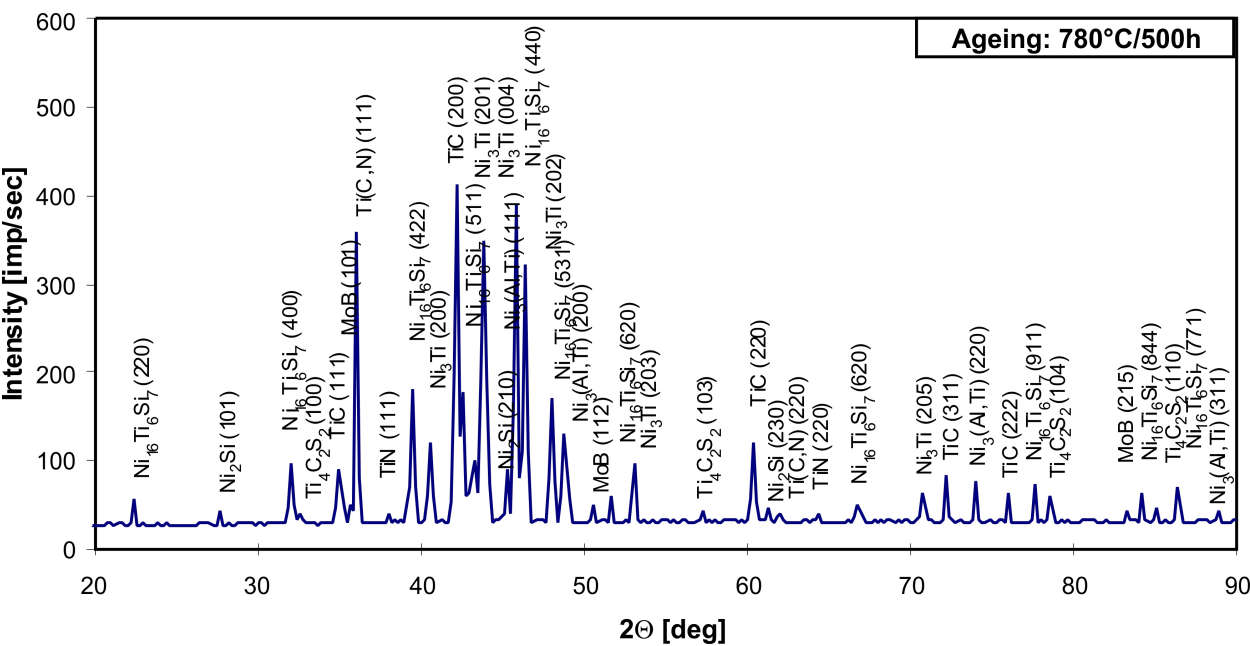

Figure 18. Isolate diffractogram of the alloy after solution heat treatment and aging at 780°C/500 h.

Alloy condition	Phase constituents
Solution heat treatment: 980°C/2 h/w	TiC; $TiC_{0,3}N_{0,7}$; $TiN_{0,3}$; $Ti_4C_2S_2$; Ni_2Si; MoB
Aging: 780°C/2 h	TiC; $TiC_{0,3}N_{0,7}$; $TiN_{0,3}$; $Ti_4C_2S_2$; Ni_2Si; MoB; G - $Ni_{16}Ti_6Si_7$; γ' - $Ni_3(Al,Ti)$
Aging: 780°C/4÷500 h	TiC; $TiC_{0,3}N_{0,7}$; $TiN_{0,3}$; $Ti_4C_2S_2$; Ni_2Si; MoB; G - $Ni_{16}Ti_6Si_7$; γ' - $Ni_3(Al,Ti)$; σ - $Cr_{0,46}Mo_{0,40}Si_{0,14}$; η - Ni_3Ti

Table 8. Phase composition of the Fe-Ni alloy isolates after solution heat treatment and aging at 780°C.

4.2. Growth kinetics of γ' phase in the Fe-Ni superalloy during prolonged aging

Observation of the microstructure by means of an electron microscope (TEM) using the thin foil technique showed that the main intermetallic phase that precipitates in the Fe-Ni alloy during aging was the γ'- Ni$_3$(Al,Ti) phase. Particles of this phase is characterized by high dispersion, precipitated homogeneously in the matrix, and a spheroidal or lenticular shape. An increase in the temperature and prolongation of the aging time caused an increase in the kinetics of their growth, coagulation, and overaging.

Quantitative analysis of the γ' phase particles that precipitated in the alloy during aging was made for aging temperatures of 715°C, 750°C and 780°C with holding times in the range of 4–500 h. The results for the selected aging times, i.e., 4 h, 150 h, 300 h, and 500 h are shown in Table 9. As can be seen in the table, in the case of aging at 715°C with holding times of 4–500 h, the average diameter of particles $\overline{D}$ grew from 7.5 nm to 28.3 nm, while the volume fraction of the particles changed within a range of 6–11%. In the case of aging at 750°C with the same holding times, an increase was observed in the average diameter of the particles from 10.6 nm to 39.5 nm, accompanied by a change in the volume fraction from 7.1% to 10.1%.

Parameter	Time of aging [h] at 715°C				Time of aging [h] at 750°C				Time of aging [h] at 780°C			
	4	150	300	500	4	150	300	500	4	150	300	500
A$_A$ [%]	10.2	14.3	14.8	16.4	11.5	15.8	16.6	15.6	9.5	13.5	13.1	11.5
$\bar{d}$ [nm]	7.4	15.7	19.6	24.6	9.2	24.4	27.0	32.1	12.7	41.2	45.0	51.2
$\overline{D}$ [nm]	7.5	17.0	22.5	28.3	10.6	28.8	32.1	39.5	13.1	45.7	52.2	58.4
V$_V$ [%]	6.0	10.3	10.4	11.1	7.1	8.6	9.4	10.1	8.1	7.7	7.8	8.4
l$_d$ [nm]	144	117	121	114	135	141	123	124	153	105	103	124

Table 9. Stereological parameters of the γ' particles in the tested Fe-Ni alloy.

When the aging temperature was the highest (780°C) with analogical holding times, the average particle diameter reached the highest values in the range from 13.1 nm to 58.4 nm, while the highest volume fraction ranged between 8.1% and 8.4%.

Examples of particle distribution histograms for the selected ageing times within the range of 4–500 h at 715–780ºC are shown in Figures 19–22. As the aging time and temperature increase, a shift can be observed of the maximum towards classes with larger diameters. This corroborates that the mean diameter $\overline{D}$ of the γ' particles increases with a longer aging time and a growing temperature of aging.

Analysis of the obtained results of stereological examination of the γ'- Ni$_3$(Al,Ti) phase particles was the basis for determining the kinetics of their growth, depending on the aging conditions of the Fe-Ni alloy (Figure 23). Based on the results from the obtained dependencies, the highest growth rate of the γ' phase particles was found at an aging temperature of 780°C, the medium rate at 750°C, and the lowest at 715°C.
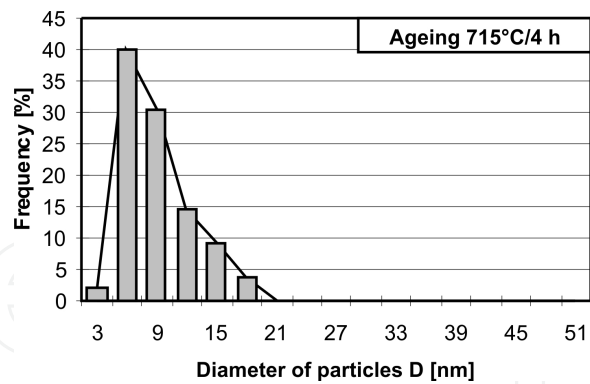
Figure 19. Distribution histogram of the diameter of γ' particles in the alloy after solution heat treatment and aging at 715°C/4 h.
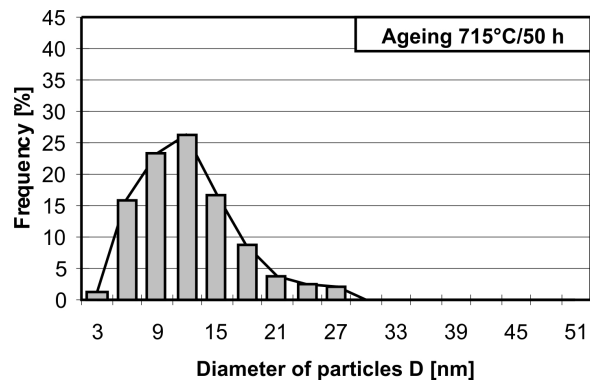
Figure 20. Distribution histogram of the diameter of γ' particles in the alloy after solution heat treatment and aging at 715°C/50 h.
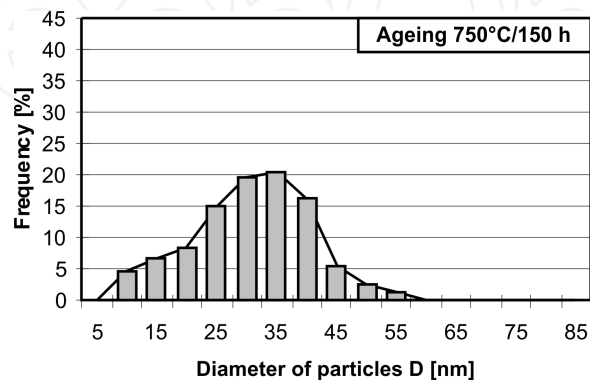
Figure 21. Distribution histogram of the diameter of γ' particles in the alloy after solution heat treatment and aging at 750°C/150 h.
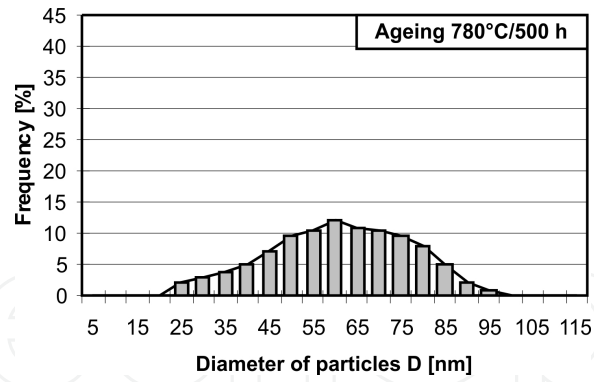
Figure 22. Distribution histogram of the diameter of γ' particles in the alloy after solution heat treatment and aging at 780°C/500 h.
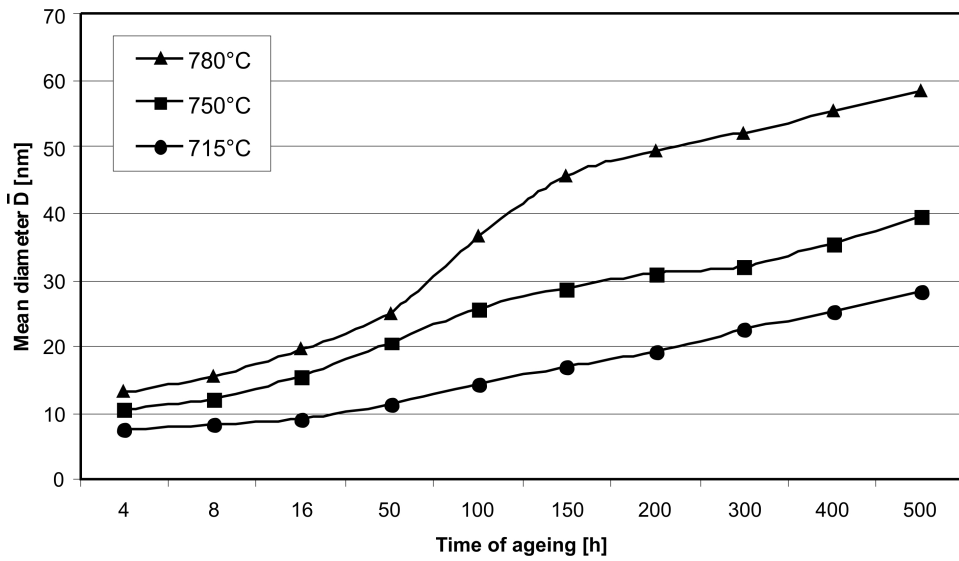

Figure 23. Dependence of the mean diameter of phase γ' precipitates in the Fe-Ni alloy on the temperature and aging time.

The analysis of the γ'- Ni$_3$(Al,Ti) phase growth step was made on the basis of the LSW theory [34,35] for coagulation on volume diffusion control according to the relationship provided by Kusabiraki et al. [36,37]:

$$\bar{d}^3 - \bar{d}_0^3 = \frac{64\sigma D C_e V_m^2}{9RT} = K't \tag{5}$$

where: $\bar{d}$ and $\bar{d}_0$ – mean diameter of the precipitates at, respectively, time t and t = 0; σ – interfacial energy between the precipitates and the matrix; D – diffusion coefficient of the solute atom in the matrix; C$_e$ – concentration of solute atoms in the matrix in equilibrium with a particle of an infinite size; V$_m$ – molar volume of the precipitation phase; R – gas constant; T – absolute temperature; K′ – growth rate constant.

The diffusion coefficient (D) can be generally expressed as:

$$D = D_0 \cdot exp\left(-E / RT\right)$$ (6)

where: D_0 – pre-exponential factor, E – activation energy of diffusion.

Hence, constant K' assumes the following form:

$$K^{'} = \frac{64\sigma D_0 C_e V_m^2 exp\left(-E / RT\right)}{9RT}$$ (7)

On assumption that the values of σ, C_e, and V_m are nearly independent of temperature, the value of diffusion activation energy (E) can be obtained from the slope of Arrhenius plot being the linear relationship between ln(TK') and T^{-1}.

The dependence of the mean diameter $\bar{D}$ of the γ' phase particles on aging time ($t^{1/3}$) and temperature is presented in Figure 24. For the analyzed aging temperature of 715÷780°C, linear dependencies were obtained, which is consistent with the LSW theory for coagulation controlled through volume diffusion. Certain deviations from the LSW theory are possible, as the theory was developed for spherical precipitates with high dispersion and a low relative volume [34, 35]. The deviation from the straight line found at a temperature of 780°C and aging time of 16÷100 h may result from breaking the γ/γ' coherence, increasing the degree of lattice mismatch between the γ' particle and the γ matrix, and in consequence, the acceleration of coagulation of the γ' phase particles. Increasing the aging temperature leads to increasing the growth and coagulation of the γ' phase particles. Values of the mean diameter of the particles $\bar{D}$ for the aging time of 0.5 h and 2 h were determined through extrapolation (Figure 24).
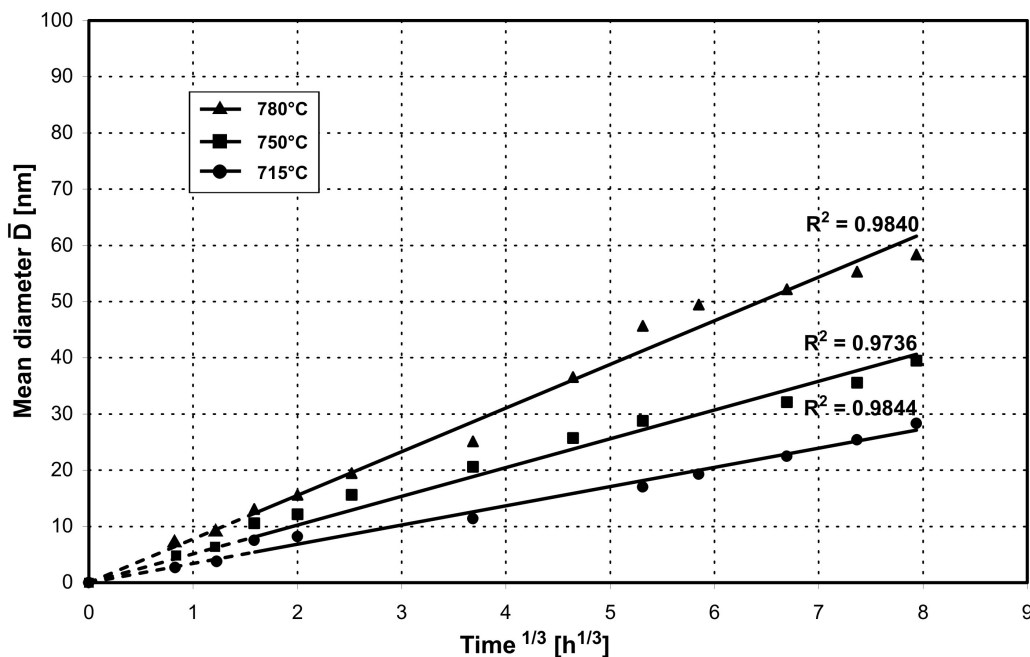

Figure 24. Dependence between the mean diameter of particles of phase γ' in the Fe-Ni alloy and the ageing time and temperature.

The activation energy of coagulation of the γ' -$Ni_3(Al, Ti)$ phase in the Fe-Ni alloy was determined from the slope of Arrhenius straight line (Figure 25) and its value (E = 297 kJ/mole) turned out to be close to that of the activation energy of phase γ' (245-298 kJ/mole), which was estimated for the chosen Fe-Ni and Ni-based superalloys [36, 37]. Moreover, the obtained value of phase γ' coagulation activation energy was close to that of the activation energy of diffusion in austenite $\curlyvee$ of the solute elements, such as Al, Ti, Ni, Fe, Cr, and Mo, which contribute to the growth of phase γ'. In the case of the examined Fe-Ni alloy, the E value showed that it was the diffusion of the solution elements that controlled the growth of phase γ', which agrees with the LSW theory.
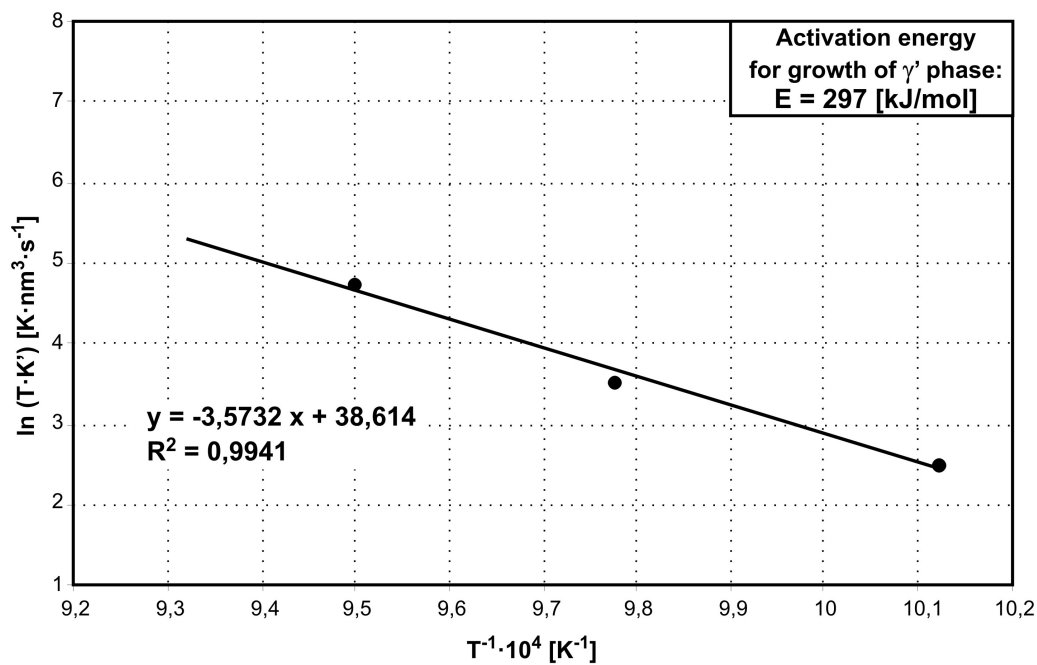
Figure 25. The plot for determination of the activation energy for coagulation process of phase γ' in the Fe-Ni alloy.

5. Summary

The analysis of the current status of the issue of wrought Fe-Ni superalloys showed that a modification of their basic chemical composition does not bring significant effects any longer. A significant improvement of technological and functional properties of Fe-Ni alloys can be obtained by introducing micro-additives that form precipitates of strengthening high-dispersion phases interacting with grain boundaries, and by applying modern manufacturing technologies that improve the quality of products. Further development of the material group of this type is closely connected with the development of wrought nickel superalloys.

The work analyzes the phase transitions and changes in the morphology of phase components of the microstructure in the selected Fe-Ni superalloy type A-286 in conditions simulating its heat treatment and operation processes. The research and analysis of its results showed a significant influence of solution heat treatment and extended aging at an elevated temperature

on the course of the precipitation process and the microstructure of the creep-resisting Fe-Ni superalloy.

After a 2-hour solution heat treatment at 980°C/water, the structure of the Fe-Ni alloy is similar to that of twinned austenite with a small content (ca. 0.3 wt. %) of undissolved precipitates of titanium compounds, such as carbide TiC, carbonitride $TiC_{0.3}N_{0.7}$, nitride $TiN_{0.3}$, carbosulfide $Ti_4C_2S_2$ and Laves phase Ni_2Si and boride MoB.

The application of a single-stage aging after solution heat treatment at temperatures of 715°C, 750°C, and 780°C with holding times from 0.5 h to 500 h causes precipitation processes of γ' - $Ni_3(Al,Ti)$, η - Ni_3Ti, β - NiTi, G - $Ni_{16}Ti_6Si_7$ and σ - $Cr_{0.46}Mo_{0.40}Si_{0.14}$ intermetallic phases in the investigated alloy, as well as the carbide $M_{23}C_6$ and boride M_3B_2.

The intermetallic γ' - $Ni_3(Al, Ti)$ phase was the main phase that precipitated during the aging of the alloy. It is possible to distinguish three characteristic stages during the γ' phase precipitation, namely: coherent zones, coherent spheroidal particles (7–25 nm), and coagulated spheroidal particles (30–60 nm). On histograms of the γ' phase size distributions, a shift can be observed of the maximum towards classes with larger diameters as the aging time and temperature increased. The volume fraction of the γ' phase particles depended on the aging time and temperature, and changed within the range of ca. 6–11%.

The mean diameter of the γ' - $Ni_3(Al, Ti)$ phase precipitates was found to increase as a function of the cube root of the aging time, which is consistent with the LSW theory claiming that coagulation is controlled by volume diffusion. In the examined alloy, the value of the γ' phase coagulation activation energy amounted to E = 297 kJ/mole and was close to the value of the solute elements' diffusion activation energy in γ-Fe, whose elements contribute to the growth of phase γ'.

The phase transition $\gamma' \rightarrow \eta$, which determines the overageing stadium of the Fe-Ni alloy, takes place through the formation of stacking faults in the structure of the γ' phase particles. A growth of the η phase lamellae proceeds in austenite in the direction <110> γ and is accompanied by the dissolution of the neighboring γ' phase particles. The η phase lamellae form the microstructure of intercrystalline Widmanstätten lamellae or precipitates in a cellular system in the regions at austenite grain boundaries.

The results of the study show that the examined Fe-Ni superalloy type A-286 has a thermally stable microstructure in the range of operation temperatures of up to ca. 700°C and therefore, it should be considered for applications in such temperatures.

Author details

Kazimierz J. Ducki

Address all correspondence to: kazimierz.ducki@polsl.pl

Silesian University of Technology, Katowice, Poland

References

[1] Sims Ch.T., Stoloff N.S., Hagel W.C. Superalloys II. New York: John Wiley & Sons; 1987.

[2] Stoloff N.S. Wrought and Powder Metallurgy (P/M) superalloys. In: ASM Handbook, editors. Volume 1, Properties and Selection: Irons, Steels, and High Performance Alloys. Materials Park, OH: ASM International; 2005. p. 1478-1527.

[3] Stickler R. Phase Stability in Superalloys. Proc. of the Symposium: High-Temperature Materials in Gas Turbines, Baden. 1973;115-146.

[4] Dulis E.J. Age-hardening austenitic stainless steels. Proc. Conference: The Metallurgical Evolution of Stainless Steels, London. 1979;420-441.

[5] Pickering F.B. Some aspects of the precipitation of nickel-aluminium-titanium intermetallic compounds in ferrous materials. Proc. Conference: The Metallurgical Evolution of Stainless Steels, London. 1979;391-401.

[6] Sourmail T. Precipitation in creep resistant austenitic stainless steels. Materials Science and Technology. 2001;17:1-14.

[7] Ducki K.J., Hetmańczyk M., Kuc D. Analysis of precipitation process of the intermetallic phases in a high-temperature Fe-Ni austenitic alloy. Materials Chemistry and Physics. 2003;81:490-492.

[8] Ducki K.J. Analysis of the precipitation and growth processes in a high-temperature Fe-Ni alloy. Journal of Achievements in Materials and Manufacturing Engineering. 2008;31:226-232.

[9] Brooks J.W., Bridges P.J.. High Temperature Alloys for Gas Turbines and other Applications. Netherlands: D. Reidl Publish. Company; 1986.

[10] Rohrbach K.P. Trends in high-temperature alloys. Advanced Materials & Processes. 1995;10:37-40.

[11] Ducki K.J. Microstructural aspects of deformation, precipitation and strengthening processes in austenitic Fe-Ni superalloy (in Polish). Gliwice, Poland: Silesian University of Technology; 2010.

[12] Ducki K.J. Fatigue behaviour and creep resistance of Fe-Ni superalloy. Saarbrücken, Germany: LAP Lambert Academic Publishing; 2014.

[13] Schubert F. Mechanische Eigenschaften von Superlegierungen und ihren Verbunden (in German). VDI Berichte. 1987;600.4:85-136.

[14] Weβling W. Festigkeitseigenschaften von Stählen für eine langzeitige Beanspruchung bei hohen Temperaturen (in German). VDI Berichte. 1987;600.4:45-84.

[15] Capdevila C., Chen Y.L., Jones A.R., Bhadeshia K.D.H. Grain Boundary Mobility in Fe-Base Oxide Dispersion Strengthened PM2000 Alloy. ISIJ International. 2003;43:777-783.

[16] Wasilkowska A., Bartsch M., Messerschmidt U., Herzog R., Czyrska-Filemonowicz A. Creep mechanism of ferritic oxide dispersion strengthened alloys. Journal of Materials Processing Technology. 2003;133:218-224.

[17] McColvin G., Munasinghe D., O'Driscoll J., Jacobs M.. Fabrication of gas turbine combustion hardware in ODS ferritic materials. In: Proc. of the 7th Liege Conference: Materials for Advanced Power Engineering; Liege. 2002. p. 833-844.

[18] Pérez P. Influence of the alloy grain size on the oxidation behaviour of PM2000 alloy. Corrosion Science. 2002;44:1793-1808.

[19] Suryanarayana C. Mechanical alloying and milling. Progress in Materials Science. 2001;46:1-184.

[20] Choudhury I.A., El-Baradie M.A. Machinability of nickel-base super alloys: A general review. Journal of Materials Processing Technology. 1998;77:278-284.

[21] Kreitner P., Appelmaier K., editors. Einfluss von Spurenelementen auf die Warmverformbarkeit von Stählen und Nickelbasis-legierungien. Spurenelemente in Stählen ed. Düsseldorf: Verlag Stahleisen; 1985. 23-34.

[22] Sczerzenie F., Maurer G.E.. Developments in Disc Materials. Materials Science and Technology. 1987;3:733-742.

[23] Härkegård G., Guédou J.Y.. Disc Materials for Advanced Gas Turbines. In: Proc. of the 6th Liége Conference: Materials for Advanced Power Engineering; Liege. 1998. p. 913-931.

[24] Pickering F.B. Physical metallurgical development of stainless steels. In: Proc. of the Conference: Stainless Steels '84; 1984; Göteborg, Sweden. 1984. p. 1-28.

[25] Schubert F.. Temperature and Time Dependent Transformation: Application to Heat Treatment of High Temperature Alloys. In: Phase Stability in High Temperature Alloys. London, UK: Appied Science Publishers Ltd; 1981. p. 119-149.

[26] Penkalla H.J., Schubert F. Ni-base wrought alloy development for USC steam turbine rotor applications. Inżynieria Materiałowa. 2004;3(140):415-421.

[27] Szala J., editor. Computer program Quantitative Metallography. Katowice, Poland: Department of Materials Science, Silesian University of Technology; 1997.

[28] Ryś J., editor. Stereology of materials (in Polish). Kraków, Poland: Fotobit Design; 1995. 394 p.

[29] Czyrska-Filemonowicz A., Dubiel B., Wiencek K.. Determination of the oxide particle density in ODS alloys by means of transmission electron microscopy. Acta Stereologica. 1998;17:225-236.

[30] Dubiel B., Wosik J., Kruk A., Penkalla H.J., Czyrska-Filemonowicz A.. Quantitative TEM microstructural analysis of Ni-based superalloy Waspaloy. In: Proceedings of the Stereology and Image Analysis in Materials Science; Kraków, Poland. Fotobit Design; 2000. p. 135-140.

[31] Schröder J.H., Arzt E.. Electron-Microscopic Investigations of Dispersion-Strength-ened Superalloys. Praktische Metallography. 1988;25:264-273.

[32] Wilson F.G. Age hardening of austenitic steels by γ'. In: Efect of second-phase parti-cles on the mechanical properties of steels. London, UK: The Iron and Steel Instytute; 1971. p. 16-21.

[33] Merrick H.F., Nicholson R.B. Some Features of Precipitation in a Nickel-Chromium-Titanium Alloy. In: Proc. 5th International Congress for Electron Microscopy; Phila-delphia. New York, USA: Academic Press; 1962. Paper K.8.

[34] Lifshitz I.M., Slyozow V.V. The kinetics of precipitation from supersaturated solid solution. Journal Phys. Chem. Solids. 1961;19:35-50.

[35] Wagner C. Theorie der Alterung von Niederschlägen durch Umlösen (Ostvald Rei-fung) (in German). Zeitschrift für Elektrochemie. 1961;65:581-591.

[36] Kusabiraki K., Takasawa Y., Ooka T. Precipitation and Growth of g' and h Phases in 53Fe-26Ni-15Cr Alloy. ISIJ International. 1995;35(5):542-547.

[37] Kusabiraki K., Zhang X., Ooka T. The Growth of γ' Precipitation in a 53Ni-20Co-15Cr Superalloy. ISIJ International. 1995;35:1115-1120.